3D Palmprint Classification by Global Features

Wei Li[b], Bob Zhang[a,c] and David Zhang[a,1]

[a]Biometric Research Center, Dept. of Computing, The Hong Kong Polytechnic University, Hong Kong, China
[b]Shenzhen Institutes of Advanced Technology, Chinese Academy of Sciences, Shenzhen, China
[c]Dept. of Electrical and Computer Engineering, University of Waterloo, Waterloo, ON, Canada

Abstract:

Three Dimensional (3D) palmprint has proved to be a significant biometrics for personal authentication. 3D palmprints are harder to counterfeit than 2D palmprints and more robust to variations in illumination and serious scrabbling on the palm surface. Previous work on 3D palmprint recognition has concentrated on local features such as texture and lines. In this paper, we propose three novel global features of 3D palmprints which describe shape information and can be used for coarse matching and indexing to improve the efficiency of palmprint recognition, especially in very large databases. The three proposed shape features are Maximum Depth (MD) of palm center, Horizontal Cross-section Area (HCA) of different levels and Radial Line Length (RLL) from the centroid to the boundary of 3D palmprint horizontal cross-section of different levels. We treat these features as a column vector and use Orthogonal Linear Discriminant Analysis (OLDA) to reduce their dimensionality. We then adopt two schemes: 1) coarse-level matching and 2) Ranking Support Vector Machine (RSVM) to improve the efficiency of palmprint recognition. We conducted a series of 3D palmprint recognition experiments using an established 3D palmprint database and the results demonstrate that the proposed method can greatly reduce penetration rates.

Keywords: 3D palmprint identification; global features; palmprint indexing; OLDA; Ranking SVM

[1] Corresponding author. Email: csdzhang@comp.polyu.edu.hk.

1. Introduction

Palmprint recognition has now been a topic of research for over ten years. Like other biometrics, palmprints demonstrate the properties required for personal authentication: universality, uniqueness, permanence, collectability and acceptability [1]. Furthermore, palmprints have some advantages over other biometrics. Palmprints are larger than fingerprints and therefore more robust to scars and dirt. Palmprint images are cheaper to collect and more acceptable than iris. Palmprints can distinguish between individuals more accurately than face and can also identify monozygotic twins [2].

Traditionally, palmprint recognition has made use of either high or low resolution 2D palmprint images. High resolution images are suitable for forensic applications [3] while low resolution images are suitable for civil and commercial applications [4]. Most current research use low resolution palmprint recognition and is either texture-based or line-based. The texture-based methods include PalmCode [4], Competitive Code [5] and Ordinal Code [6]. These methods use a group of filters to enhance and extract the phase or directional features which can represent the texture of the palmprint. Line-based methods use line or edge detectors to explicitly extract line information from the palmprint that is then used for matching. The representative methods include Derivative of Gaussian based line extraction [7] and Modified Finite Radon transform (MFRAT) based line extraction [8].

In recent years, 3D techniques have been applied to biometric authentication, such as 3D face [9] and 3D ear recognition [10]. Most recently, a structured-light imaging [11, 12] 3D palmprint system [13] was developed that captures the depth information of a palmprint. This information is then used to calculate the Mean and the Gaussian curvatures for use in 3D palmprint matching and recognition. To date, however, there has been no work with 3D palmprints that has extracted global shape features, which may be useful in classification and indexing. For fingerprint, according to the global ridge structure and singularities, it can be classified into five classes: arch, tented arch, left loop, right loop and whorl [14]. Wu et al. classified the palmprint into six classes according to the

palmprint principal lines [15]. Besides the exclusive classification technique, the continuous classification technique is also widely used for indexing the database for personal identification [16].

In this paper, we propose extracting three novel global features from a 3D palmprint image: Maximum Depth (MD) at the center of the palm, Horizontal Cross-section Area (HCA) at different levels of the palm; and Radial Line Length (RLL) measured from the centroid to the boundary of the 3D palmprint. These features are then used to describe and classify the shape of the 3D palmprint using continuous classification. This involves first reducing the dimensionality of the features by treating these features as a column vector and applying Orthogonal Linear Discriminant Analysis (OLDA) [17]. We then improve the efficiency of palmprint recognition by indexing the database using coarse-level matching and Ranking Support Vector Machine (RSVM) [18]

The rest of the paper is organized as follows. Section 2 describes how we define a region of interest for the 3D palmprint image and then extract our three proposed global features. Section 3 describes how global features can be used in classification in order to speed up identification. Section 4 gives the experimental results and Section 5 concludes the paper.

2. Global Features: Definitions and Extraction

The following describes our procedure for first extracting a region of interest from the 3D palmprint and then from that extract our proposed three global features.

2.1 The Region of Interest

Our definition and extraction procedure makes use of a 3D palmprint image containing 768×576 points captured using a structured-light imaging based 3D palmprint acquisition device [13]. First, we remove redundant and noisy boundary regions using a very simple Region of Interest (ROI) extraction process (Fig. 1). We segment a 400×400 points square that is respectively 68, 108, 234 and 134 points from the top, bottom, left and right boundaries of the 3D palmprint image as shown in Fig. 1 (a). Fig. 1 (b) shows the extracted ROI. After downsampling the 3D ROI to 200×200

points, we store it in a 200 by 200 matrix, $\{d_{ij} | i = 1, 2, \cdots, 200;\ j = 1, 2, \cdots, 200.\}$, where d_{ij} is the depth value of the i^{th} row and j^{th} column point of the 3D ROI.

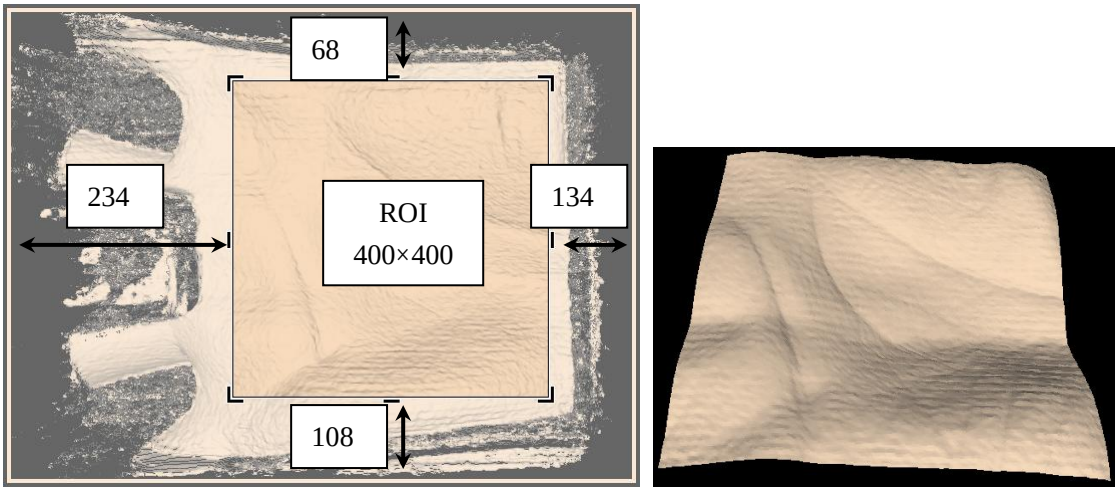

(a) (b)

Figure 1. The ROI extraction of 3D palmprint. (a) The location of the ROI in the 3D palmprint image; (b) the extracted 3D ROI.

Our proposed 3D palmprint ROI extraction approach is much simpler than the one reported in [4] and the extracted shape features are not sensitive to translation and rotation, which is why we can use such a coarse ROI extraction. As the shape feature is a form of global feature, we extract as large an ROI as possible. Of course, such a large ROI may contain noisy data so we use a mask to remove the noisy data according to the gradient of the 3D data. If the gradient of the point, which is defined as $|\nabla d| = \sqrt{\left(\frac{\partial d}{\partial x}\right)^2 + \left(\frac{\partial d}{\partial y}\right)^2}$, is larger than a given threshold, the point is regarded as noisy data. Fig. 2 shows a 3D ROI which contains noisy data and its corresponding mask. We use a 200 by 200 matrix, $\{m_{ij} | i = 1, 2, \cdots, 200;\ j = 1, 2, \cdots, 200.\}$, to represent the mask, where $m_{ij} = 0$ is noisy data and $m_{ij} = 1$ is for other data.

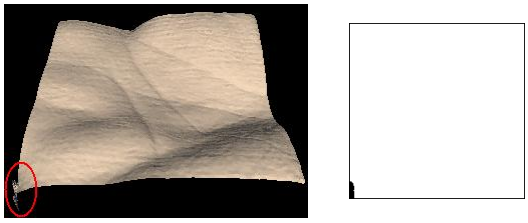

(a) (b)

Figure 2. (a) 3D ROI with noise; (b) Mask of the 3D ROI.

2.2 Three Global Features

Using the ROI obtained from the original 3D palmprint data, we extract three kinds of features to describe the shape of the 3D palmprint: Maximum Depth (MD) of palm center, the Horizontal Cross-section Area (HCA) of different levels and the Radial Line Length (RLL) from the centroid to the boundary of 3D palmprint horizontal cross-section of different levels.

2.2.1 Maximum Depth (MD)

MD means the maximum depth value of the 3D palm from a reference plane. The reference plane is decided using a rectangle as shown in the left of Fig. 3 (a). The depth of the reference plane d_r is the mean depth of the points contained by this rectangle.

$$d_r = \frac{1}{\sum_{i=R_s}^{R_e}\sum_{j=C_s}^{C_e} m_{ij}} \sum_{i=R_s}^{R_e}\sum_{j=C_s}^{C_e} (d_{ij} \cdot m_{ij}) \tag{1}$$

where d_{ij} is the depth value of the i^{th} row and j^{th} column point of the 3D ROI, m_{ij} is the corresponding mask value, R_s, R_e, C_s and C_e respectively denote the start row, end row, start column and end column. The parameters $R_s = 65$, $R_e = 136$, $C_s = 6$ and $C_e = 35$ were set by experience. The reason we choose this region is that in the 3D ROI it appears to be relatively flat.

After getting the depth of the reference plane, we find the maximum depth, $d_{\max}$, in a region denoted by the right rectangle in Fig. 3 (a) which starts at the 41^{st} row and extends to the 160^{th} row and from the 65^{th} column to the 190^{th} column. The MD can then be calculated easily by (2) as shown in Fig. 3 (b).

$$MD = d_{\max} - d_r \tag{2}$$

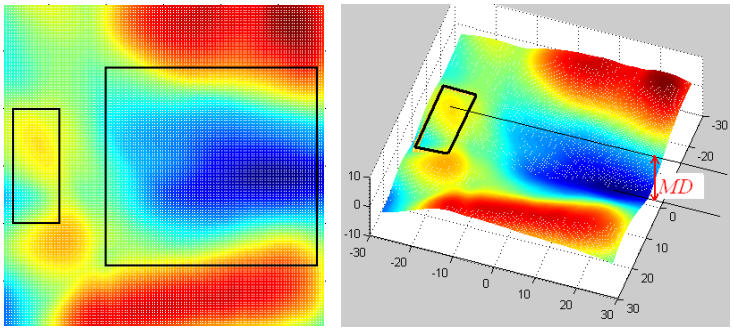

(a) (b)

Figure 3. Illustration of the MD feature (with color denoting the depth of the 3D ROI). (a) Location of the two rectangles used to calculate the reference plane and to find the maximum depth point; (b) Illustration of the MD feature.

2.2.2 Horizontal Cross-section Area (HCA)

To describe the shape of the 3D palmprint, we use a group of equidistant horizontal planes to cut the 3D ROI as shown in Fig. 4. Fig. 5 shows a 3D ROI and its contour cut by the equidistant horizontal planes. To render the shape clearly, Fig. 5 (a) only shows the 3D ROI image and hides the equidistant horizontal planes. In Fig. 5 (b), the blue curves denote deeper levels, the red curves denote higher levels and the remainder are medium levels. The HCA is defined as the area enclosed by the level curve. From Fig. 5 (b), we can see that most of the deeper level curves are enclosed and the areas are simply connected. These are more stable in response to noise or transformation.

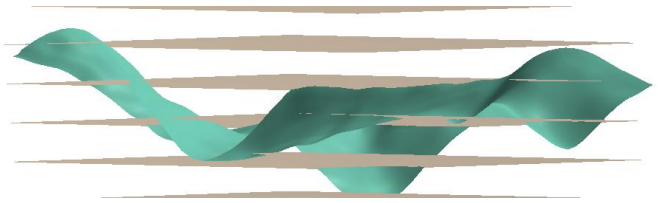

Figure 4. Illustration of the 3D ROI crossed by horizontal planes.

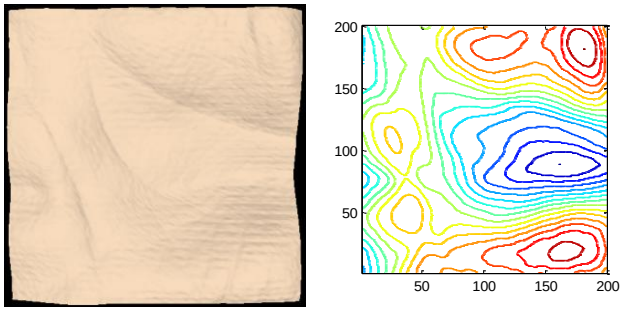

(a) (b)

Figure 5. (a) A 3D ROI; (b) Its corresponding contour cutting by the equidistant horizontal planes.

To get a stable HCA, we take into consideration only the levels from the deepest point to the reference plane, defined in section 3.1. Suppose we divide this region into N levels. Every level $G^k, k=1,2,\cdots,N$ is described with a 200×200 matrix and calculated by (3).

$$G_{ij}^k = \begin{cases} 1, if\ d_{ij} > h\cdot(N-k+1)/N \\ 0, \qquad\qquad others \end{cases}, k=1,2,\cdots,N; i=1,2,\cdots,200;\ j=1,2,\cdots,200. \tag{3}$$

where d_{ij} is the depth value of the i^{th} row and j^{th} column point of the 3D ROI and h is the palmprint depth defined by (2).

To make it more stable, we constrain every level growing from its previous level except the first level. That is

$$L^k = G^k \cap (L^{k-1} \oplus \Theta^{k-1}), \quad k=2,3,\cdots,N; L^1 = G^1. \tag{4}$$

where "$\cap$" denotes logical AND, $\oplus$ denotes a morphological dilation operation and Θ^k is a disk morphological structuring element whose size can be calculated by $35-3\times k$ (this is suitable for N = 8 by experience).

Fig. 6 shows an example of all the levels stacked together. Fig. 7 shows each of the levels separately.

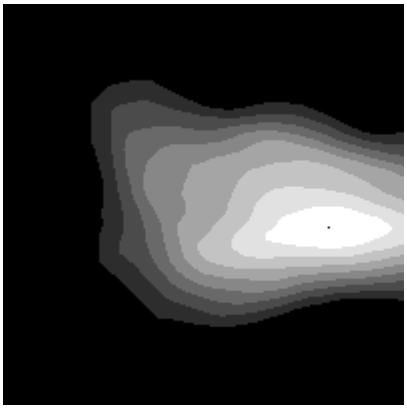

Figure 6. An example of all the levels stacked together when N = 8.

After getting the cross-sectional levels $L^k, k=1,2,\cdots,N$, the HCA, $A^k, k=1,2,\cdots,N$ can be easily calculated by

$$A^k = \sum_{i=1}^{200}\sum_{j=1}^{200} L_{ij}^k \tag{5}$$

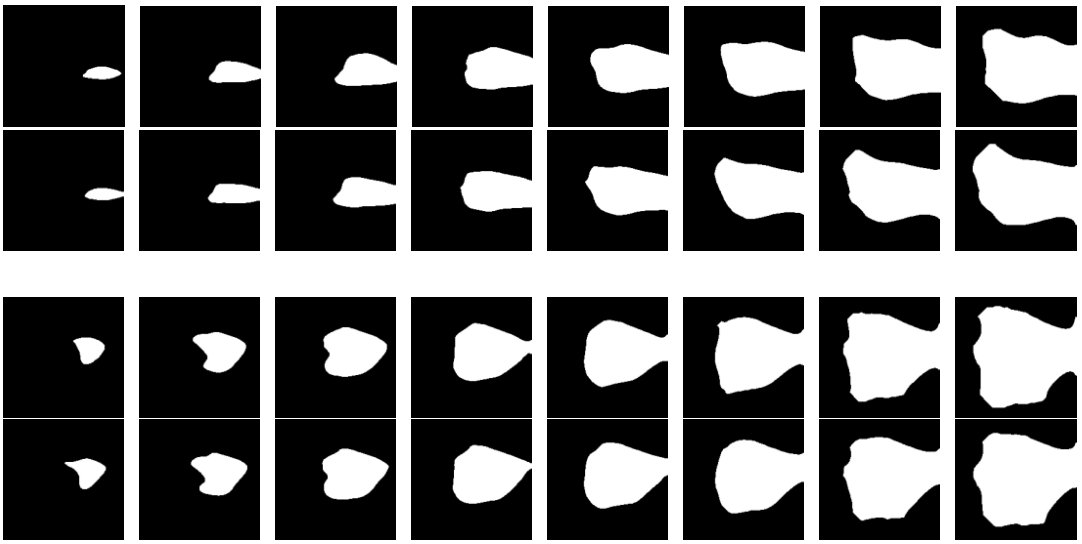

Figure 7. The cross-sectional area feature (the top two rows are extracted from two samples collected from one palm; and the bottom two rows are extracted from two samples from another palm).

2.2.3 Radial Line Length (RLL)

The HCA is only a coarse description of the cross-section. To identify samples which have a similar cross-sectional area but have a different contour, we propose the RLL feature which describes the shape of the contour. First, we calculate the centroid of the first level L^1, thereafter we treat it as the centroid of all levels. Then, from the centroid we draw M radial lines which intersect with the contour of every level. The distance between the intersection and the centroid is defined as the RLL. The radial lines are distributed at equal angles. We record these radial lines from the inner layers to the outer layers starting with the horizontal direction by an $M \times N$ dimensional vector, $R_i, i = 1, 2, \cdots, M \times N$, where M is the number of radial lines and N is the number of cross-sections. Fig. 8 shows some examples of radial lines and their cross-sections. We can see that the RLL better represents the contour as the number of radial lines increases.

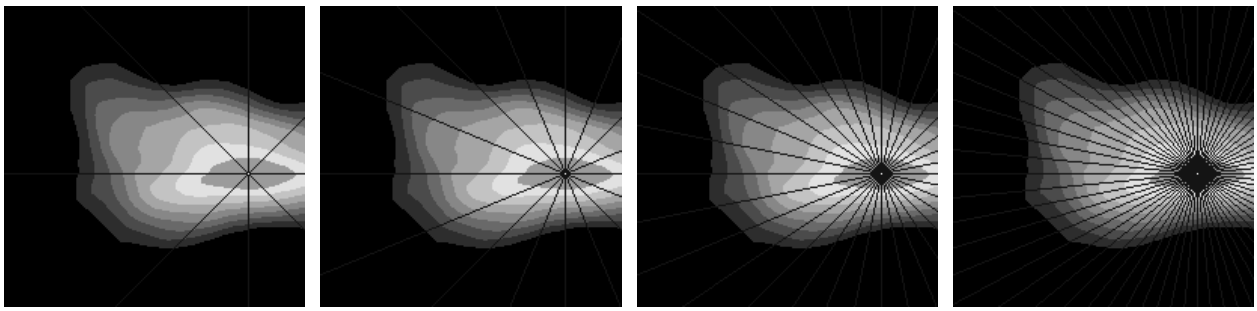

Figure 8. Radial line starting from the centroid (from left to right, M = 8, 16, 32 and 64 respectively).

The above three global features are mainly determined by the central region of the palm. This region is certainly contained by the ROI described in Section 2.1 which makes these features insensitive to translation and rotation. Although the RLL feature can be affected by rotation as the contours change smoothly, if the rotation is small then the variation of the RLL feature will also be small. Actually, there are some restricting pegs on the capture device which can guide the user to put his/her hand on the proper place as described in [13]. Furthermore, we assume the user is cooperative when collecting data as we aim at civil rather than law enforcement applications.

3. Classification with Global Features

The classification of biometrics speeds up the identification process by reducing the number of comparisons that must be made. There are two kinds of classification techniques: exclusive classification and continuous classification. Both fingerprint [14] and palmprint classifications [15] make use of exclusive classification. The main problem of this technique is that it uses only a small number of classes and the samples are unevenly distributed between them, with more than 90% of the samples being in just two or three classes. A further problem with exclusive classification is that when classification is performed automatically, it is necessary to handle errors and rejected samples gracefully, which is a hard problem in practice. In contrast, for continuous classification, samples are not partitioned into disjoint classes but rather associated with numerical vectors which represent features of the samples. These feature vectors are created through a similarity-preserving transformation so that similar samples are mapped into close points in the multi-dimensional space [19]. In this paper, we adopt the continuous classification technique. As the global features combining MD, HCA and RLL are high-dimensional, we reduce the dimensions using the LDA method. We then improve the efficiency of palmprint recognition by applying coarse-level matching and Ranking Support Vector Machine (RSVM) to the low dimensional vectors.

3.1 Dimension reduction using orthogonal LDA

LDA is a state-of-the-art dimensionality reduction technique widely used in classification problems. The objective is to find the optimal projection which simultaneously minimizes the within-class distance and maximizes the between-class distance, thus achieving maximum discrimination (Here, the "class" is used to denote the identity of the subjects, e.g. the samples collected from one palm are regarded as one class). However, the traditional LDA requires the within-class scatter matrix to be nonsingular, which means the sample size should be large enough compared with its dimension, but is not always possible. In this paper, we therefore adopt the orthogonal LDA (OLDA) proposed in [17], where the vectors of the optimal projection are calculated using the training database and the optimal projecting vectors are orthogonal to each other.

Suppose the 3D ROI has been divided to N levels and that M radial lines are used to represent the level contours. We can list the global features as a column vector, $F = \left\{ MD, A^1, A^2, \cdots, A^N, R^1, R^2, \cdots, R^{N\times M} \right\}$, with $1+N+N\times M$ rows. Given a training database which has n samples and k classes as $X = [X_1, X_{2,} \cdots, X_k]$, where $X_i \in \mathbb{R}^{(1+N+N\times M)\times n_i}$, $i = 1, 2, \cdots, k$ and $n = \sum_{i=1}^{k} n_i$, adopting OLDA [17] the optimal projection W can be calculated as follows.

First, the within-class scatter matrix S_w, the between-class scatter matrix S_b and total scatter matrix S_t can be expressed as

$$S_w = H_w H_w^T, S_b = H_b H_b^T, S_t = H_t H_t^T \tag{6}$$

where

$$H_w = \frac{1}{\sqrt{n}} \left[X_1 - m_1 \cdot e_1^T, \cdots, X_k - m_k \cdot e_k^T \right] \tag{7}$$

$$H_b = \frac{1}{\sqrt{n}} \left[\sqrt{n_1}(m_1 - m), \cdots, \sqrt{n_k}(m_k - m) \right] \tag{8}$$

$$H_t = \frac{1}{\sqrt{n}}(X - m \cdot e^T) \tag{9}$$

where m_i is the centroid of the i^{th} class X_i, m is the centroid of all the training samples X, $e_i = [1,1,\cdots,1]^T \in \mathbb{R}^{n_i}$, $i = 1,2,\cdots,k$ and $e = [1,1,\cdots,1]^T \in \mathbb{R}^n$.

After calculating H_w, H_b and H_t, the reduced Singular Value Decomposition (SVD) is applied to H_t.

$$H_t \xrightarrow{\text{Reduced } SVD} U_r \Sigma_r V_r^T \tag{10}$$

Denote $B = \Sigma_r^{-1} U_r^T H_b$ and compute the SVD of *B*.

$$B \xrightarrow{SVD} U_B \Sigma_B V_B^T \tag{11}$$

Let

$$D = U_r \Sigma_r^{-1} U_B \tag{12}$$

$$q = rank(B) \tag{13}$$

and denote D_q the first q columns of the matrix D. Then, compute the QR decomposition of D_q.

$$D_q \xrightarrow{QR\ decomposition} QR \tag{14}$$

where *Q* is the desired orthogonal matrix and optimal projection, i.e. $W = Q$.

After getting the optimal projection *W*, we can map the $1 + N + N \times M$ dimensional vector *F* to a lower dimensional space

$$\tilde{F} = W^T F \tag{15}$$

where $\tilde{F} = \{f_1, f_2, \cdots, f_\Gamma\}$ is a Γ dimensional vector with $\Gamma < 1 + N + N \times M$.

3.2 Coarse-level matching

As the purpose of coarse-level matching is to speed up the identification during retrieval, we can regard it as a continuous classification approach. After mapping the global features' Γ dimensional vector $\tilde{F}$, the global features can be used to measure the similarity of two samples as

follows:

$$\Delta = \left\| \tilde{F}^1 - \tilde{F}^2 \right\|_2 = \sum_{i=1}^{\Gamma} (\mathrm{f}_i^1 - \mathrm{f}_i^2)^2 \tag{16}$$

In 3D palmprint identification, we can use the Γ dimensional global features to carry out coarse-level matching as shown in Fig. 9. If the testing sample passes coarse-level matching, it undergoes fine-level matching using 3D palmprint local features. If it does not pass, it moves on to the next sample in the database and so on until it has accessed the last sample in the database. From (16), we can see that coarse-level matching requires only Γ times of addition and multiplication which is much faster than fine-level matching using local features. Eq. (17) gives the fine-level matching by Mean Curvature Image (MCI) feature [13]:

$$Y = \frac{2\sum_{i=1}^{n}\sum_{j=1}^{m} Z_d(i,j) \cap Z_t(i,j)}{\sum_{i=1}^{n}\sum_{j=1}^{m} Z_d(i,j) + \sum_{i=1}^{n}\sum_{j=1}^{m} Z_t(i,j)} \tag{17}$$

where symbol "$\cap$" represents the logical AND operation, Z_d and Z_t are the two binarized MCI features. To deal with the translation problem of ROI when calculating the matching score by (17), we will shift two, four, six and eight pixels of the test image along 8 directions: right, left, up, down, left-up, left-down, right-up and right-down, respectively. Adding the non-shift one, we will have $8\times 4+1=33$ matching scores and the maximum one is selected. Suppose the size of the MCI feature is 128×128, i.e. $m=128$ and $n=128$, from (16) and (17) we can see that coarse-level matching is much faster than fine-level matching.

3.3 Ranking Support Vector Machine (RSVM)

Coarse-level matching scheme is a simple and easy way to reduce retrieval times. It's more useful for palmprint recognition if we can rank the candidate samples in the database in descending order according to the above global features. Searching for the closest matches to a given query vector in a large database is time consuming if the vector is even moderately high-dimensional. Various methods have been proposed to speed up the nearest neighbor retrieval, including hashing and tree

structures [20]. However, the complexity of these methods grows exponentially with increasing dimensionality [21]. Therefore, we have adopted the Ranking Support Vector Machine (RSVM) method [18], inspired by the approaches of internet search engines, to rank the candidate samples in the database.

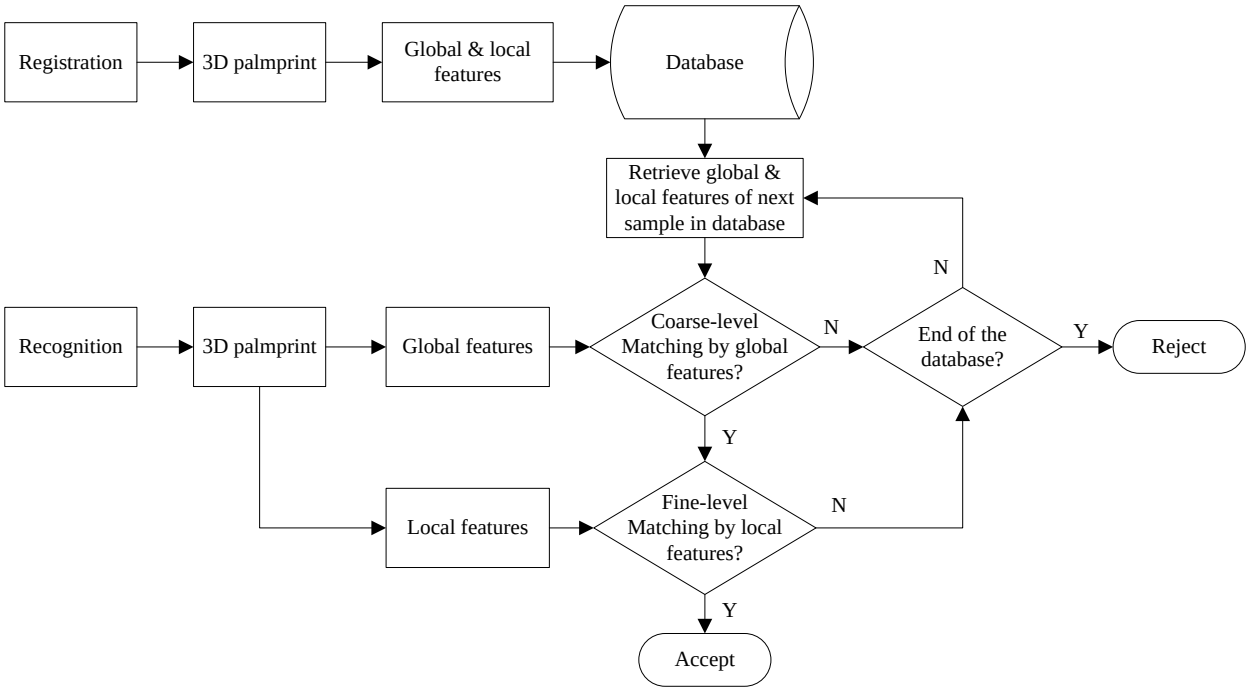

Figure 9. The flowchart of registration and recognition with coarse-level matching scheme.

Given a query $q_k, k=1,2,\cdots,n$ and a sample collection $D=\{d_1,d_2,\cdots,d_m\}$, the optimal retrieval system should return a ranking $r_k^*, k=1,2,\cdots,n$ that orders the samples in *D* according to their relevance to the query. In this paper, the query q and the sample d are the Γ dimensional global features as described above. In our approach, if a sample d_i is ranked higher than d_j in some ordering r, i.e. $r(d_i)>r(d_j)$, then $(d_i,d_j)\in r$, otherwise $(d_i,d_j)\notin r$. Consider the class of linear ranking functions

$$(d_i,d_j)\in f_{\vec{w}}(q)\Leftrightarrow \vec{w}\phi(q,d_i)>\vec{w}\phi(q,d_j) \tag{18}$$

where $\vec{w}$ is a weighted vector that is adjusted by learning and $\phi(q,d)$ is a mapping onto features that describe the match between q and d which can be defined as $\phi(q,d)=\|q-d\|_2$. Our goal is to find the optimal ranking function that will satisfy the maximum number of the following

inequalities.

$$\begin{aligned} &\forall (d_i, d_j) \in r_1^* : \vec{w}\phi(q_1, d_i) > \vec{w}\phi(q_1, d_j) \\ &\quad \cdots \\ &\forall (d_i, d_j) \in r_n^* : \vec{w}\phi(q_n, d_i) > \vec{w}\phi(q_n, d_j) \end{aligned} \tag{19}$$

It is easier to solve this problem if it is converted into to the following SVM classification problem by introducing non-negative slack variable $\xi_{i,j,k}$.

Hence, the problem is to minimize:

$$V(\vec{w}, \vec{\xi}) = \tfrac{1}{2}\vec{w} \cdot \vec{w} + C\sum \xi_{i,j,k} \tag{20}$$

subject to:

$$\begin{aligned} &\forall (d_i, d_j) \in r_1^* : \vec{w}\left(\phi(q_1, d_i) - \phi(q_1, d_j)\right) \geq 1 - \xi_{i,j,1} \\ &\quad \cdots \\ &\forall (d_i, d_j) \in r_n^* : \vec{w}\left(\phi(q_n, d_i) - \phi(q_n, d_j)\right) \geq 1 - \xi_{i,j,n} \end{aligned} \tag{21}$$

$$\forall i \forall j \forall k : \xi_{i,j,k} \geq 0 \tag{22}$$

where C is a parameter that allows trading-off margin size against training error and $C = 0.1$ set by experience.

In the training stage, it is the inner-class samples of a test sample that should be ranked higher than the inter-class samples, e.g. inner-class samples rank is 1 and inter-class samples rank is 0. We input the ranks together with the Γ dimensional global features into the RSVM algorithm to learn the optimal ranking function $f_{\vec{w}^*}$. Given a new query q, the samples in the database can be sorted by their value of

$$rsv(q, d_i) = \vec{w}^* \phi(q, d_i) \tag{23}$$

4. Experimental Results

We used the 3D palmprint acquisition device developed in [13] to establish a 3D palmprint database containing 8000 samples collected from 400 palms. The 3D palmprint samples were

collected in two separated sessions, 10 samples in each session. The average time interval between the two sessions is one month. The collection procedure required volunteers to put their palms naturally and without force on the device. The original spatial resolution of the data was 768×576. After ROI extraction, the central part (400×400) was extracted and downsampled to (200×200) for feature extraction and recognition.

The database was divided into a training part (the first session of 4000 samples) and a testing part (the second session of 4000 samples). As described in Section 3, the dimension of the proposed global features is $1+N+N\times M$. To select the value of M and N we carried out a series of verifications on the training database where the class of the input palmprint was known. Each of the 3D samples was matched with the remaining samples in the training database. A successful match is where the two samples are from the same class. This is referred to as intra-class matching and the candidate image is said to be genuine. An unsuccessful match is referred to as inter-class matching and the candidate image is said to be an impostor. Treating the global features as a point in the $1+N+N\times M$ dimension space, we simply use the Euclidian distance as the matching score. Table 1 shows the Equal Error Rate (EER) for $N=4,8,16$ and $M=8,16,32,64$. The best result is $N=8$ and $M=32$.

In order to balance accuracy and efficiency, we chose $N=8$ and $M=32$ in the following experiments. This means the global features have $1+N+N\times M=265$ dimensions. Table 2 shows the verification results by MD, HCA, RLL and their combined results. From the last column of Table 2 we can see using the combined three global features will achieve a lower EER than each of the individual features. As described in section 3.1, we use the OLDA method to reduce global features to a lower Γ dimension. To decide the optimal value of Γ, we carried out a series of recognition experiments on the 4000 sample training database. We divided this database into two equal parts and then chose the first five samples of every palm for training and set aside the rest for testing. As shown in section 3.1, Γ is equal to q in (13). Instead of $q=rank(B)$, we let $q=1,2,\cdots,10,12,15,20,30$. Table 3 and Fig. 10 show the recognition results. We can see that 15

dimensions is a good choice for the following coarse-level matching and RSVM schemes.

Table 1. The EER of 3D palmprint verification for $N = 4,8,16$ and $M = 8,16,32,64$ by MD+HCA+RLL.

	M = 8 EER (%)	M = 16 EER (%)	M = 32 EER (%)	M = 64 EER (%)
N = 4	14.30	19.15	14.35	14.07
N = 8	14.20	16.30	12.32	12.54
N = 16	18.11	18.35	15.21	14.11

Table 2. The EER of 3D palmprint verification for $N = 8$ and $M = 32$ by MD, HCA, RLL and their combined result.

Global features	MD	HCA	RLL	MD+HCA+RLL
EER(%)	25.8	20.4	18.6	12.32

Table 3. 3D palmprint recognition rate by OLDA for different dimensions.

Γ	1	2	3	4	5	6	7	8	9	10	12	15	20	30
Recognition rate (%)	2.0	9.6	26.0	42.6	56.6	66.2	74.6	78.4	82.4	83.8	86.0	89.6	90.4	93.6

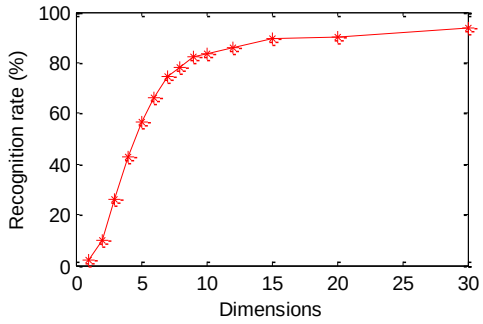

Figure 10. The plot of 3D palmprint recognition rate by OLDA for different dimensions.

Fig. 11 shows the genuine and imposter distributions when the 3D palmprint 15-dimensional global features are applied to the 4000 samples in the training database. Figs. 11 (a) to (o) are obtained by using the Euclidian distance to match the single dimension value from the 1st to 15th. Fig. 11 (p) shows the result of using the Euclidian distance to match all 15 dimensional values.

We next carried out the 3D palmprint classification and recognition experiments using the first sample of each class in the training database as a template and the 4000 samples in the testing database as probes, making a total of 400 templates and 4000 probes. The performance of classification and recognition is usually measured by error rate and penetration rate calculated in

[19] as follows:

$$\text{error rate}=\frac{\text{number of false match}}{\text{total number of probe}}\times 100\% \tag{24}$$

$$\text{penetration rate} = \frac{\text{number of accessed template}}{\text{total number of template in the database}}\times 100\% \tag{25}$$

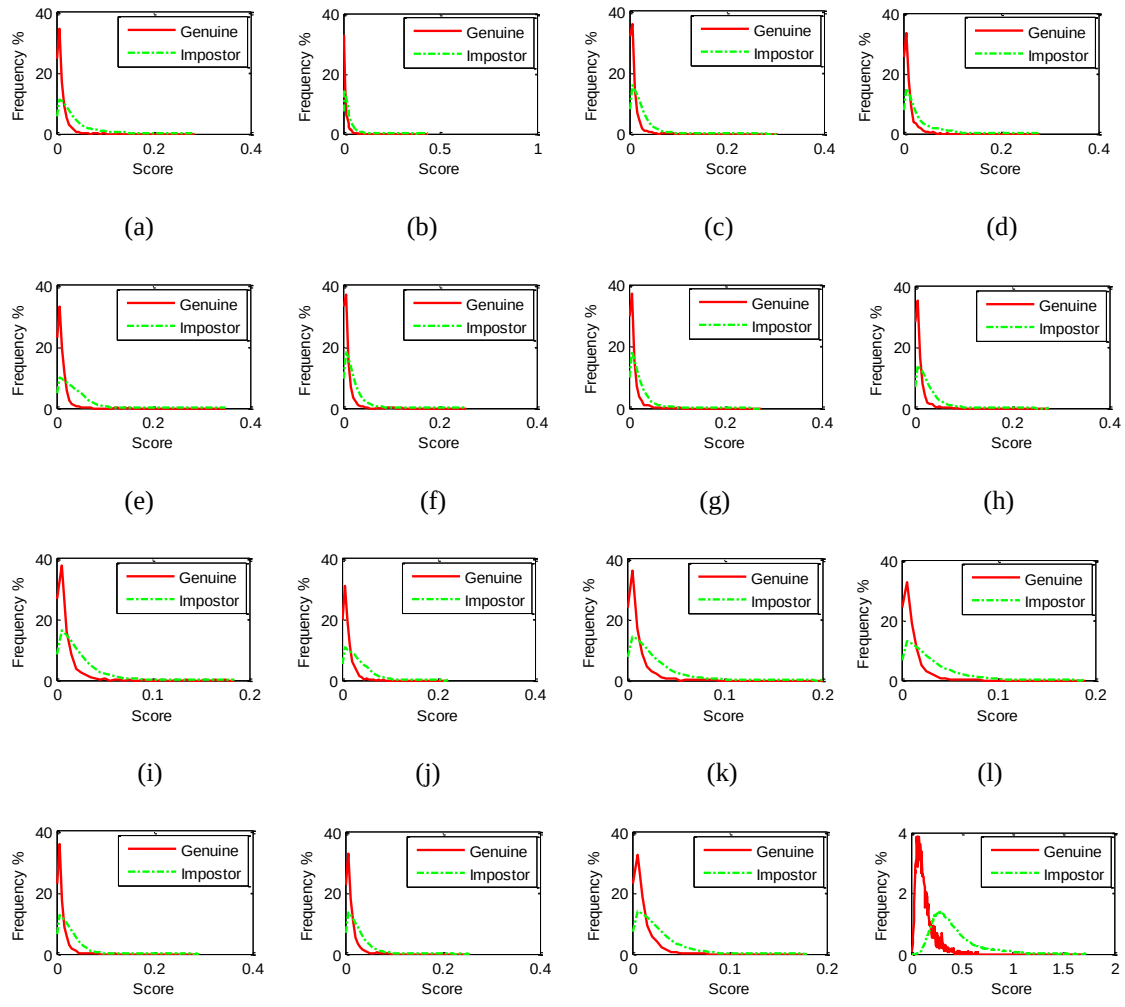

Figure 11. Genuine and imposter distributions by the 3D palmprint 15-dimensional global features. (a) to (o) are obtained by matching the single dimension value from the 1st to 15th and (p) is obtained by matching all 15 dimensional values together.

Obviously there is a trade-off between error rates and penetration rates. Generally speaking, if there is no classification, there are two retrieval strategies: 1) all of the templates in the database are visited and the template that gives the best matching score is regarded as the matched template, if the matching score is less than a given threshold Ψ_T; 2) given a threshold Ψ_t, the search

continues until a match is found that is below that threshold.

We used three 3D palmprint recognition matching approaches: 1) no classification; 2) coarse-level matching; and 3) RSVM. For no classification, we matched using the local feature MCI as described in [13]. The process we used for coarse-level matching is illustrated in Fig. 9 and involves fine-level matching using the local feature MCI. A single instance of coarse-level matching requires only 1/36000 of the time it takes to do fine-level matching (coarse-level matching only needs 15 operations while fine-level matching must do $128\times128\times(8\times4+1)$ operations, where 128×128 is the size of ROI and $8\times4+1$ is the shifting template times). For the above two approaches, the penetration rate and the error rate will vary with different thresholds Ψ_t. As for RSVM, we use the RSVM algorithm described in section 3.3 to rank the templates in the database, and then match the top ρ percent by local feature MCI with the best matching score regarded as the matched template if this score is less than a given constant threshold Ψ_T. We can see from (25) that the ρ is equal to the penetration rate. Given different thresholds Ψ_t and ρ, we carried out a series of 3D palmprint recognition experiments. Table 4, Table 5 and Fig. 12 show these experimental results. Even at an approximately equal error rate, the proposed coarse-level matching and RSVM approaches get a much lower penetration rate than the no classification approach. Obviously RSVM has the best performance but requires an additional offline training process compared to coarse-level matching.

Table 4. Performance comparison of the three 3D palmprint recognition approaches.

No classification		Coarse-level matching		RSVM	
Penetration rate (%)	Error rate (%)	Penetration rate (%)	Error rate (%)	Penetration rate (%)	Error rate (%)
100*	1.29	45.2	1.31	30	1.30
51.1	1.68	41.6	1.32	27.5	1.33
49.3	1.86	38.8	1.36	25	1.37
47.2	2.10	34.7	1.42	22.5	1.42
45.9	2.33	29.1	1.56	20	1.49
43.7	2.60	23.5	1.78	17.5	1.63
42.6	2.95	20.5	2.12	15	1.87
41.5	3.30	18.4	2.39	12.5	2.48
40.3	3.75	13.3	3.16	10	3.35
38.1	4.80	10.1	4.30	7.5	4.41
35.9	5.86	8.6	5.79	5	5.88

* This row used retrieval strategies 1) and the remaining rows used retrieval strategies 2) for no classification.

Table 5. Running time comparison of the three 3D palmprint recognition approaches.

	Once feature extraction time	Once dimensionality reduction time	Ranking or coarse matching time for all templates in database	Once matching time by MCI	Total running time for one probe testing
No classification	112ms	0ms	0ms	0.86ms	112+0.86*400*1.0 = 456ms
Coarse-level matching	136ms	0.1ms	0.5ms	0.86ms	136+0.1+0.5+0.86*400*0.452 = 292.09ms
RSVM	136ms	0.1ms	1.56ms	0.86ms	136+0.1+1.56+0.86*400*0.30 =240.86ms

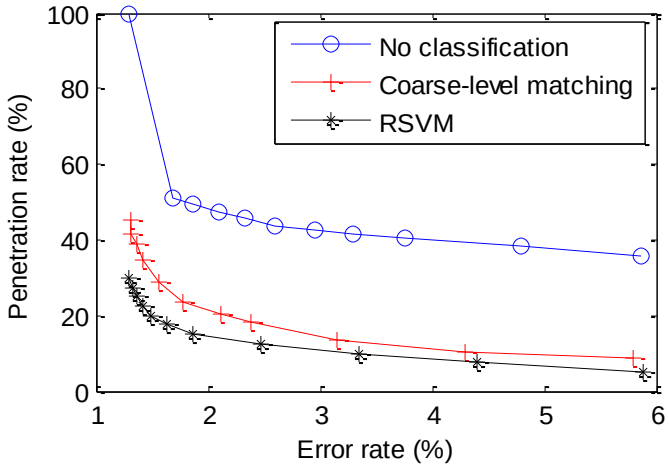

Figure 12. Plot of the penetration rate and error rate of the three 3D palmprint recognition approaches.

5. Conclusion

This paper proposed three global features for 3D palmprint images: Maximum Depth (MD), Horizontal Cross-section Area (HCA) and Radial Line Length (RLL). These cannot be extracted from 2D palmprints and are not correlated with local features, such as line and texture features. To make these global features efficient for use in coarse classification, we treat them as a multi-dimensional vector and use OLDA to map it to a lower dimensional space. We then improve the efficiency of 3D palmprint recognition using two proposed approaches, coarse-level matching and RSVM, both of which significantly reduce the penetration rate during retrieval. Our recognition experiments using an established 3D palmprint database of 8,000 samples show that the global features improve palmprint classification which greatly reduces search times.

Acknowledgements

The authors would like to thank the editor and the anonymous reviewers for their help in improving the paper. The work is partially supported by the GRF fund from the HKSAR Government, the central fund from Hong Kong Polytechnic University, and the NSFC Oversea fund (61020106004), China.

References

[1] R.M. Bolle, J.H. Connell, S. Pankanti, N.K. Ratha, and A.W. Senior, *Guide to Biometrics*, Springer, U.S., 2003.

[2] A.W.K. Kong, D. Zhang, and G.M. Lu, "A study of identical twins' palmprints for personal verification," *Pattern Recognition*, vol. 39, no. 11, pp. 2149-2156, April 2006.

[3] A. K. Jain and J.J. Feng, "Latent Palmprint Matching," *IEEE Transactions on Pattern Analysis and Machine Intelligence*, vol. 31, no. 6, pp. 1032-1047, 2009.

[4] D. Zhang, A.W.K. Kong, J. You, and M. Wong, "On-line palmprint identification," *IEEE Transactions on Pattern Analysis and Machine Intelligence*, vol. 25, no. 9, pp. 1041-1050, 2003.

[5] A.W.K. Kong and D. Zhang, "Competitive coding scheme for palmprint verification," *Proceedings of International Conference on Pattern Recognition*, vol. 1, pp. 520-523, 2004.

[6] Z.N. Sun, T.N. Tan, Y.H. Wang, and S.Z. Li. "Ordinal palmprint representation for personal identification," *Proceeding of IEEE International Conference on Computer Vision and Pattern Recognition*, pp. 279-284, 2005.

[7] X.Q. Wu, D. Zhang, and K.Q. Wang, "Palm line extraction and matching for personal authentication," *IEEE Transactions on Systems, Man and Cybernetics, Part A*, vol. 36, no. 5, pp. 978-987, Sept. 2006.

[8] D.S. Huang, W. Jia, and D. Zhang, "Palmprint verification based on principal lines," *Pattern Recognition*, vol. 41, no. 4, pp. 1316-1328, April 2008.

[9] C. Samir, A. Srivastava, and M. Daoudi, "Three-dimensional face recognition using shapes of facial curves," *IEEE Transactions on Pattern Analysis and Machine Intelligence*, vol. 28, no. 11, pp. 1858-1863, Nov. 2006.

[10] P. Yan and K.W. Bowyer, "Biometric recognition using 3D ear shape", *IEEE Transactions on Pattern Analysis and Machine Intelligence*, vol. 29, no. 8, pp. 1297-1308, Aug. 2007.

[11] V. Srinivassan and H.C. Liu, "Automated phase measuring profilometry of 3D diffuse object," *Appl. Opt.*, vol. 23, no. 18, pp. 3105-3108, 1984.

[12] H.O. Saldner and J.M. Huntley, "Temporal phase unwrapping: application to surface profiling of discontinuous objects," *Appl.Opt.*, vol. 36, no. 13, pp. 2770-2775, 1997.

[13] D. Zhang, G. Lu, W. Li, L. Zhang, and N. Luo, "Palmprint Recognition Using 3-D Information," *IEEE Transactions on Systems, Man, and Cybernetics, Part C: Applications and Reviews*, vol. 39, no. 5, pp. 505-519, Sept. 2009.

[14] E. Henry, *Classification and Uses of Finger Prints*, Routledge, London, 1900.

[15] X.Q. Wu, D. Zhang, K.Q. Wang, and B. Huang, "Palmprint classification using principal lines," *Pattern Recognition*, vol. 37, no. 10, pp. 1987-1998, 2004.

[16] A. Lumini, D. Maio, and D. Maltoni, Continuous vs. Exclusive Classification for Fingerprint Retrieval," *Pattern Recognition Letters*, vol. 18, no. 10, pp. 1027-1034, 1997.

[17] J.P. Ye, "Characterization of a Family of Algorithms for Generalized Discriminant Analysis on Undersampled Problems," *Journal of Machine Learning Research*, vol. 6, pp. 483-502, 2005.

[18] T. Joachims, "Optimizing Search Engines Using Clickthrough Data," *Proceedings of the eighth ACM SIGKDD international conference on Knowledge discovery and data mining*, pp. 133-142, 2002.

[19] D. Maltoni, D. Maio, A.K. Jain, and S. *Prabhakar, Handbook of Fingerprint Recognition,* Springer, U.S., 2003.

[20] B. Matei, Y. Shan, H. Sawhney, Y. Tan, R. Kumar, D. Huber, and M. Hebert, "Rapid Object Indexing Using Locality Sensitive Hashing and Joint 3DSignature Space Estimation," *IEEE Transactions on Pattern Analysis and Machine Intelligence*, vol. 28, no. 7, pp. 1111-1126, July 2006.

[21] H. Chen and B. Bhanu, "Efficient Recognition of Highly Similar 3D Objects in Range Images," *IEEE Transactions on Pattern Analysis and Machine Intelligence*, vol. 31, no. 1, pp. 172-179, 2009.